

PNNL-32364

NRAP-Open-IAM Multisegmented Wellbore Reduced-Order Model

Quality Assurance

November 2021

Seunghwan Baek
Diana H Bacon
Nicolas J Huerta

DISCLAIMER

This report was prepared as an account of work sponsored by an agency of the United States Government. Neither the United States Government nor any agency thereof, nor Battelle Memorial Institute, nor any of their employees, makes **any warranty, express or implied, or assumes any legal liability or responsibility for the accuracy, completeness, or usefulness of any information, apparatus, product, or process disclosed, or represents that its use would not infringe privately owned rights.** Reference herein to any specific commercial product, process, or service by trade name, trademark, manufacturer, or otherwise does not necessarily constitute or imply its endorsement, recommendation, or favoring by the United States Government or any agency thereof, or Battelle Memorial Institute. The views and opinions of authors expressed herein do not necessarily state or reflect those of the United States Government or any agency thereof.

PACIFIC NORTHWEST NATIONAL LABORATORY
operated by
BATTELLE
for the
UNITED STATES DEPARTMENT OF ENERGY
under Contract DE-AC05-76RL01830

Printed in the United States of America

Available to DOE and DOE contractors from the
Office of Scientific and Technical Information,
P.O. Box 62, Oak Ridge, TN 37831-0062;
ph: (865) 576-8401
fax: (865) 576-5728
email: reports@adonis.osti.gov

Available to the public from the National Technical Information Service
5301 Shawnee Rd., Alexandria, VA 22312
ph: (800) 553-NTIS (6847)
email: orders@ntis.gov <<https://www.ntis.gov/about>>
Online ordering: <http://www.ntis.gov>

NRAP-Open-IAM Multisegmented Wellbore Reduced-Order Model

Quality Assurance

November 2021

Seunghwan Baek
Diana H Bacon
Nicolas J Huerta

Prepared for
the U.S. Department of Energy
under Contract DE-AC05-76RL01830

Pacific Northwest National Laboratory
Richland, Washington 99354

Abstract

Geologic carbon storage is one of the promising strategies to mitigate climate change by reducing the emission of carbon dioxide to the atmosphere. As part of the National Risk Assessment Partnership (NRAP), a systems-level stochastic analysis tool called the open source integrated assessment model, NRAP-Open-IAM, has been developed to estimate and manage the risk of containment loss at a geological carbon sequestration site. NRAP-Open-IAM contains several wellbore leakage model components that estimate the fluid leak rate that may occur through compromised legacy wells due to the increase in pressure resulting from CO₂ injection activities. Coupled to a reservoir component model, these components estimate the leakage of CO₂ and/or brine from a storage reservoir to overlying aquifer layers and the atmosphere through legacy wells. This report presents the theoretical framework and quality testing of the multisegmented wellbore reduced-order model. The model allows for segmenting of the legacy wells passing through the overlying stratigraphy into several intervals to simulate a site's specific stratigraphic and hydrogeologic properties. For quality assurance, the analytical model is validated against numerical reservoir flow simulations for single and multiple aquifer(s) models. The results indicate that the model accurately predicts the transport of two-phase fluids (brine and injected CO₂) through the well over time. A detailed description of the model helps users to understand the model and provides a basis for future improvements.

Acknowledgments

This work was completed as part of the U.S. Department of Energy's (DOE's) National Risk Assessment Partnership (NRAP) project, supported by the DOE Office of Fossil Energy's Cross-Cutting Research Program. The work was performed by Pacific Northwest National Laboratory under DOE contract number DE-AC05-76RL01830.

Acronyms and Abbreviations

DOE	U.S. Department of Energy
GCS	geological carbon sequestration
MAE	mean absolute error
MSW	multisegmented wellbore
NRAP	National Risk Assessment Partnership
NRAP-Open-IAM	NRAP's open source integrated assessment model
ROM	reduced-order model
STOMP	Subsurface Transport Over Multiple Phases
UIC	Underground Injection Control

Contents

Abstract.....	iii
Acknowledgments.....	iv
Acronyms and Abbreviations.....	v
1.0 Introduction	1
2.0 Methodology.....	3
2.1 Numerical Simulation: STOMP-CO ₂ E	4
2.2 Multisegmented Wellbore ROM derivation	5
3.0 Results and Discussion	15
3.1 Model Validation	15
3.2 Multiple Layer Model Applications.....	16
4.0 Conclusion	19
5.0 References.....	20
Appendix A – Input file of STOMP for a Benchmark Problem.....	A.1
Appendix B – Case Study with the Default Number of Aquifers.....	B.1

Figures

Figure 1. Diagram of the quality assurance workflow for the multisegmented wellbore ROM.	3
Figure 2. Single aquifer model configuration: a) diagram of the cross-sectional schematic and b) map view of the STOMP mesh and well locations for the benchmark problem used for validation. Dimensions are in meters.....	4
Figure 3. Model stratigraphy of MSW.....	6
Figure 4. Validation of STOMP model.....	15
Figure 5. Coupled MSW ROM validation against STOMP results: a) brine leakage mass rate into aquifer 1 from the storage reservoir; b) CO ₂ leakage mass rate into aquifer 1 from the storage reservoir. STOMP-CO ₂ E result (yellow) on the right subplot is identical to that in Figure 4. Log time is used for both x-axes. The NRAP model (i.e., MSW ROM) is shown in red (modified version) and blue (original version). The secondary y-axis (right side) calculates the absolute difference.	16
Figure 6. Multiple layer model with four aquifers and five shale layers.	17
Figure 7. Inflow mass rate comparison. Red: STOMP, blue: NRAP. Top row: CO ₂ , bottom row: brine.	18
Figure 8. Cumulative mass comparison. Red: STOMP, blue: NRAP.....	18

Tables

Table 1. Numerical model parameters for the benchmark problem.	5
Table 2. Residual brine saturation used for the multiple layer model.	17

1.0 Introduction

Geologic carbon storage (GCS) is one technology that could be used to help mitigate climate change by injecting carbon dioxide into the subsurface and thereby reduce the emission of carbon dioxide to the atmosphere. Several pilot-scale GCS projects in the U.S. and across the world have demonstrated this technology's feasibility (Yokonfski et al. 2019). The technology is supported by the many decades of experience with subsurface oil and gas production, waste water injection, gas storage, and geothermal operations.

Within the U.S., CO₂ injection activities are overseen by the U.S. Environmental Protection Agency, and the Class VI regulations within the Underground Injection Control (UIC) regulation are designed to protect underground sources of drinking water with strict requirements for the operation and post-management of GCS (Bacon et al. 2020). Safe operation of a GCS site requires quantitative estimates of the site's long-term performance that consider not only subsurface hydrologic, geochemical processes and interactions resulting from CO₂ injection and movement, but also, and as importantly, the related uncertainties. Thus, a modeling approach that can efficiently couple component models for various aspect of a GCS site and can allow rapid computation is desired (Pawar et al. 2016). As part of the National Risk Assessment Partnership (NRAP) tool development effort, in 2017, the team released a set of 10 tools (i.e., the NRAP Toolset) that can be used to estimate risks associated with GCS (NETL 2021). Within the toolset, uncertainties in storage reservoirs, leakage scenarios, and shallow groundwater impacts are effectively considered in a stochastic framework. A set of component models, comprising either analytical models or physics-based reduced-order models (ROMs), enable rapid probabilistic risk assessments. These tools are developed to help regulators and operators understand potential risks amidst uncertainties in their GCS operations.

Wells are often considered high-risk pathways for fluid leakage in a CO₂ sequestration site due to defects caused by either poor well completion or subsequent damage arising from chemical reactions and thermal and/or mechanical stresses (Gasda et al. 2004). The NRAP-Open-IAM contains several wellbore model components [e.g., open wellbore model (Bacon et al. 2021), cemented wellbore model (Jordan et al. 2015), multisegmented wellbore (MSW) model] that estimate the impacts of the unlikely event that leakage occurs from existing penetrations to the reservoir, the injection well, and any associated monitoring wells during and after GCS operations.

This report presents the testing of the MSW ROM. The analytical component model was originally proposed in Nordbotten et al. (2004 and 2009) and applied for risk assessment in the presence of multiple overlying aquifers or thief zones for field scale GCS applications. This model analyzes leakage of CO₂ and brine from a storage reservoir where CO₂ is injected, to the overlying layers through legacy wells relying on a one-dimensional multiphase version of Darcy's law. The model assumes that the leak occurs in a compromised cemented annulus, for example, between the outside of the casing and borehole. The leak path contains alternating well segments, which are set with a length and an effective permeability value for the flow path. The segmented leak path allows for approximating vertical heterogeneity and having varying permeability formations the fluid may leak into (e.g., the primary seal or underground source of drinking water). When incorporated into the NRAP-Open-IAM, this leakage model can be coupled to site-specific reservoir model simulations or aquifer ROMs for stochastic risk assessments. As part of NRAP-Open-IAM's software quality assurance plan, this model must be qualified. Here, for quality assurance, the model is described in detail, and its predictive capability is compared with the numerical reservoir flow simulation for single and multiple

aquifer(s) models. This work provides readers with a better understanding of the working principle, capabilities, and limitations of the model.

2.0 Methodology

This section describes the overall quality assessment process (Figure 1). For quality assurance of the MSW ROM, a reference calculation is required for comparison with a more accurate model. In this report, the reference calculations are numerical simulations performed using the Subsurface Transport Over Multiple Phases (STOMP) code, a multi-phase flow simulator developed by Pacific Northwest National Laboratory (White et al. 2012). STOMP is used to create full subsurface simulations (i.e., a system containing a storage reservoir, a leaky well, and one or more aquifers for fluid to leak into), which are used as the basis for comparison with the MSW model.

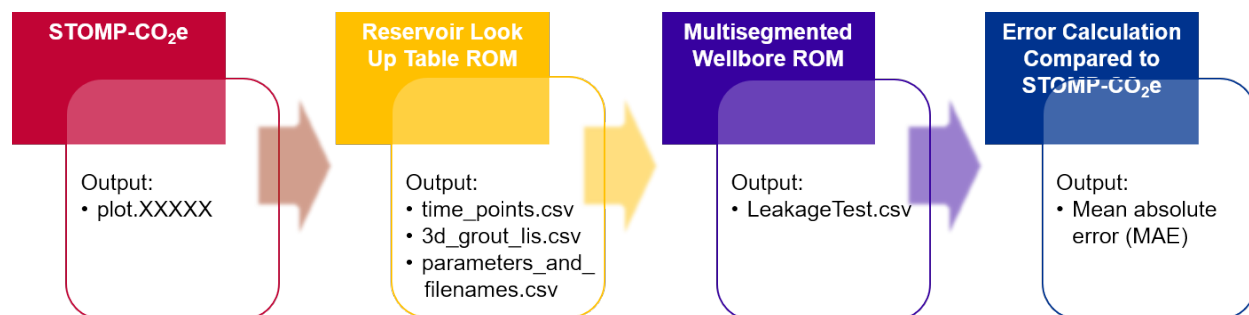


Figure 1. Diagram of the quality assurance workflow for the multisegmented wellbore ROM.

The MSW ROM needs to be coupled with another component model to provide the input signals needed to drive leakage, which provides pressure and saturation at timesteps and at specific wells locations. In the current version of NRAP-Open-IAM (Vasylykivska et al. 2021), the input model can be either the Analytical Reservoir component (Baek et al. 2021) or a reservoir lookup table component. For this analysis, we use the storage reservoir for the full system STOMP simulations as the reservoir lookup table component.

The reservoir lookup table component extracts user-specified information for each cell at discrete timesteps of a selected layer of the model from the STOMP output files (*plot.XXXXX*) and converts it into the table format needed for the NRAP-Open-IAM. Specifically, the file “*time_points.csv*” includes user-specified timestep information, and “*3d_grout_lis.csv*” has comma-delimited pressure and saturation information for targeted cells, extracted from the STOMP output (i.e., *plot.XXXXX*). The file “*Parameters_and_filenames.csv*” has information on the types of the parameters varied for stochastic analysis and filenames for each set of them. In this study, the stochastic analysis is not conducted, so a dummy file is used. “*time_points.csv*” and “*3d_grout_lis.csv*” serve as input data, and the data is interpolated to provide reservoir pressure and saturation at user-defined locations and time to the MSW ROM.

The MSW ROM takes the inputs and calculates the brine and CO₂ leakage from the storage reservoir to overlying aquifers and/or the atmosphere (i.e., the surface) (Vasylykivska et al. 2021). This ROM links several NRAP-Open-IAM models and allows the user to investigate potential risks associated with leakage scenarios (e.g., a plume intersecting an abandoned leaky well) that may occur during GCS.

Since the STOMP results are used for the reservoir component, via the reservoir lookup table ROM (i.e., pressure and saturation at a leaky well in reservoir), it is assumed that differences

between the STOMP outputs and the MSW ROM outputs are attributed to the MSW ROM's model assumptions and limitations.

2.1 Numerical Simulation: STOMP-CO₂E

As a reference for the MSW ROM, a numerical simulation model is built using STOMP and a benchmark problem introduced in Class et al. (2009). The model configurations are shown in Figure 2. For quality assurance purposes we use two GCS scenarios, one with a single aquifer and one with multiple aquifer models, for comparison.

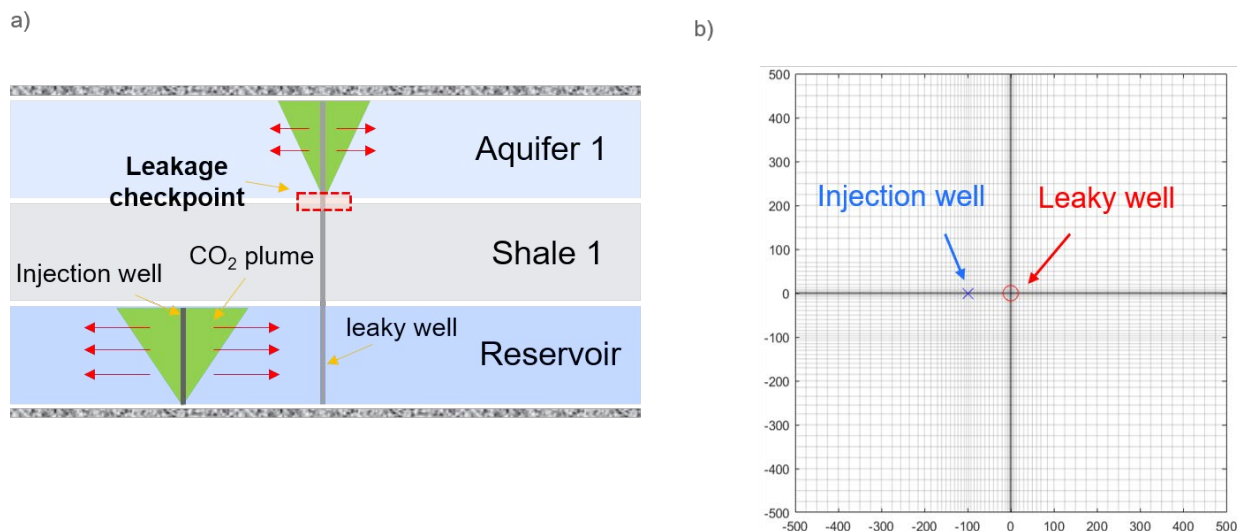


Figure 2. Single aquifer model configuration: a) diagram of the cross-sectional schematic and b) map view of the STOMP mesh and well locations for the benchmark problem used for validation. Dimensions are in meters.

The benchmark problem consists of a 3D model (Figure 2a) with the storage reservoir (thickness: 30 m) at the bottom where CO₂ is injected through an injection well, and one shale layer (thickness: 100m) in the middle, which is considered impermeable, and one leaky well passes through. The aquifer (thickness: 30 m) sits at the top of the model, and the brine and CO₂ leakage are monitored at the leakage checkpoint, which is located between the top of the shale and the bottom of the aquifer (Figure 2a). The leak rates at the leakage checkpoint are measured for comparison with literature (Class et al. 2009) and provide the main point of comparison for quality assurance purposes. A map view of the mesh generated for the model reservoir is shown in Figure 2b.

For reliability and speed of the numerical simulation, tartan grids were adopted focusing (i.e., highly discretized) around the leaky well and injection wells. The leaky well is located at the center of the mesh (i.e., x-coordinate: 0 m, y-coordinate: 0 m), and the grids at the leaky well are discretized with the effective cross-sectional area of the well. The x- and y- dimensions of the square grid at the well locations are 0.266 m, which is calculated based on the 0.15 m radius of a cylindrical well. The injection well is located 100 m away from the grid (i.e., x-coordinate: -100 m, y-coordinate: 0 m), and a fully coupled wellbore model (Peaceman 1983) is used with a radius of 0.15 m. It is assumed that the well is connected to all cells at the well location across the reservoir. At the well location, the grid dimensions in x and y are 5 m.

The STOMP model is initially fully brine saturated, and the residual brine saturation was set at zero for the entire domain. The residual brine saturation is the fraction of irreducible volume occupied by brine. Thus, the maximum pore volume fraction of the injected CO₂ is 1–residual brine saturation. For multiphase fluid flow, linear (i.e., x-type) relative permeability curves were used, and capillary pressure is negligible. The model case assumes that fluid properties such as viscosity and density are constant, all processes are isothermal, and mutual dissolution between CO₂ and brine is negligible. Thus, no changes in density and viscosity associated with CO₂ injection were considered. The fluids were considered incompressible and rock pore volume in all layers was considered near incompressible (1.0×10^{-12} 1/Pa). Hydrostatic pressure gradient is assumed at 9.8 MPa/km, and each formation layer (i.e., reservoir, shale 1, aquifer 1) is homogeneous and isotropic. A constant pressure boundary condition (Dirichlet) is applied for all lateral boundaries, and the top and bottom of the model are sealed, leading to no vertical flow communication. The simulation parameters are summarized in Table 1, and STOMP input is included in Appendix A.

Table 1. Numerical model parameters for the benchmark problem.

Parameter	Units	Value
CO ₂ density	kg/m ³	479
Brine density	kg/m ³	1,045
CO ₂ viscosity	Pa-sec	3.95×10^{-5}
Brine viscosity	Pa-sec	2.54×10^{-4}
Reservoir permeability	m ²	2.0×10^{-14}
Reservoir bottom depth	m	3,000
Reservoir thickness	m	30
Shale 1 thickness	m	100
Aquifer 1 thickness	m	30
Leaky well permeability ^(a)	m ²	1.0×10^{-12}
Porosity ^(b)	-	0.15
Mass injection rate	kg/s	8.87
Distance between wells	m	100
Dimensions of model domain	m	1,000 × 1,000 × 30
Simulation time	days	1,000

(a) Leaky well permeability is independent to the permeability of each layer. In the model, the permeabilities of the shale 1 and aquifer 1 layers are not defined.
(b) Porosity of all grids in the model (i.e., reservoir and wellbore)

2.2 Multisegmented Wellbore ROM derivation

The MSW ROM component in NRAP-Open-IAM (Vasylykivska et al. 2021) was developed to calculate leakage from the injection layer through wells across formations based on the model developed by Nordbotten et al. (2004, 2009). The model needs a reservoir model (e.g., reservoir lookup table model or analytical reservoir model) as input to provide the pressure at the top of the reservoir and vertically averaged saturation in the reservoir at the leaky well location over time. This section elaborates on the implemented equations.

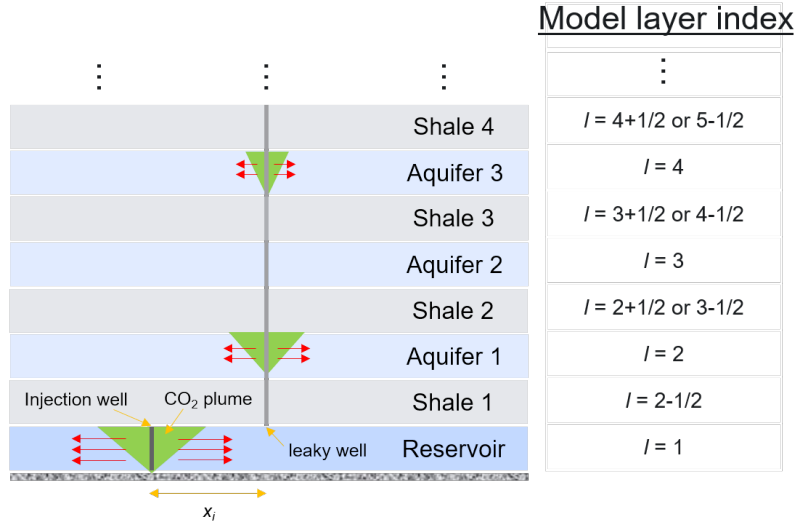


Figure 3. Model stratigraphy of MSW.

In this particular system, the pressure change is caused by the net effects of the inflow mass into the system and outflow mass out of the system (Nordbotten et al. 2004). Conceptually, thus, the pressure change can be considered the sum of the pressure changes at each location. The pressure change $\Delta P^{l,t}(x_i)$ at a location x_i (i.e., the distance from the injection well location) at timestep t in comparison to the initial pressure (i.e., $t = 0$) in aquifer l is expressed as

$$\Delta P^{l,t}(x_i) = \Delta P_{in}^{l,t}(x_i) + \Delta P_{out}^{l,t}(x_i) \quad (1)$$

where $\Delta P_{in}^{l,t}(x_i)$ is pressure perturbation in aquifer l driven by the fluid supply from the below aquifer $l-1$, $\Delta P_{out}^{l,t}(x_i)$ is pressure perturbation in aquifer l driven by the fluid leakage out of aquifer l to the above aquifer $l+1$ at timestep t . Refer to Figure 3 for the model layer index. Note that the index for the aquifer starts from $l = 2$, and the total number of the aquifers in the model is $n-1$.

$\Delta P_{in}^{l,t}(x_i)$ and $\Delta P_{out}^{l,t}(x_i)$ consist of the pressure change by each phase fluid, α and β (throughout the report, α and β indicate CO_2 and brine, respectively) as

$$\Delta P^{l,t}(x_i) = \{\Delta P_{in,\alpha}^{l,t}(x_i) + \Delta P_{in,\beta}^{l,t}(x_i)\} + \{\Delta P_{out,\alpha}^{l,t}(x_i) + \Delta P_{out,\beta}^{l,t}(x_i)\} \quad (2)$$

$\Delta P_{in,\alpha}^{l,t}(x_i)$ is calculated as

$$\Delta P_{in,\alpha}^{l,t}(x_i) = \dot{Q}_{in,\alpha}^{l,t}(x_i) \frac{W(u)}{4\pi\Lambda_{aq}^{l,t-1}h_{aq}^l K_{h,aq}^l} \quad (3)$$

where $\dot{Q}_{in,\alpha}^{l,t}(x_i)$ is inflow mass rate of the phase α from the underlying aquifer $l-1$ to aquifer l at timestep t , r_{wi} is the injection well radius, h_{aq}^l is the thickness of aquifer l , $K_{h,aq}^l$ is the horizontal permeability of aquifer l and effective (volume-weighted) mobility, $\Lambda_{aq}^{l,t-1}$ is calculated based on saturation in the previous step $t-1$ as (Nordbotten and Celia 2012)

$$\Lambda_{aq}^{l,t-1} = S_{\alpha}^{l,t-1} \left(\frac{k_{r,\alpha}^{l,t-1}}{\mu_{\alpha}^l} \right) + (1 - S_{\alpha}^{l,t-1}) \frac{k_{r,\beta}^{l,t-1}}{\mu_{\beta}^l} \quad (4)$$

where $S_{\alpha}^{l,t-1}$, $k_{r,\alpha}^{l,t-1}$, and μ_{α}^l are the saturation, relative permeability, and viscosity of phase α in aquifer l , respectively. $k_{r,\beta}^{l,t-1}$ and μ_{β}^l are the relative permeability and viscosity of phase β in aquifer l , respectively. The relative permeability is dependent on the saturation from the previous step; thus, it is denoted as $k_{r,\alpha}^{l,t-1}$, $k_{r,\beta}^{l,t-1}$. The subscript aq is used for aquifer.

Well function, $W(u)$ in Eq. (3), is used to represent the perturbation in pressure by fluid transport and calculated as (Bear 1979)

$$W(u) = -0.5772 - \ln u + u - \frac{u^2}{2 \cdot 2!} + \frac{u^3}{3 \cdot 3!} - \frac{u^4}{4 \cdot 4!} + \frac{u^5}{5 \cdot 5!} - \frac{u^6}{6 \cdot 6!} + \frac{u^7}{7 \cdot 7!} - \frac{u^8}{8 \cdot 8!} \dots \quad (5)$$

where

$$u = \frac{r_{wi}^2 c_{f,\beta}}{4\Lambda_{aq}^{l,t-1} K_{h,aq}^l (0.92 * \sum time)} \quad (6)$$

where $c_{f,\beta}$ is fluid compressibility of the phase β .

Similarly,

$$\Delta P_{in,\beta}^{l,t}(x_i) = \dot{Q}_{in,\beta}^{l,t}(x_i) \frac{W(u)}{4\pi\Lambda_{aq}^{l,t-1} h_{aq}^l K_{h,aq}^l} \quad (7)$$

$$\Delta P_{out,\alpha}^{l,t}(x_i) = \dot{Q}_{out,\alpha}^{l,t}(x_i) \frac{W(u)}{4\pi\Lambda_{aq}^{l,t-1} h_{aq}^l K_{h,aq}^l} \quad (8)$$

$$\Delta P_{out,\beta}^{l,t}(x_i) = \dot{Q}_{out,\beta}^{l,t}(x_i) \frac{W(u)}{4\pi\Lambda_{aq}^{l,t-1} h_{aq}^l K_{h,aq}^l} \quad (9)$$

where $\dot{Q}_{out,\alpha}^{l,t}(x_i)$ and $\dot{Q}_{out,\beta}^{l,t}(x_i)$ are outflow mass rate of the phase α and β , respectively, from aquifer l to $l+1$ at timestep t .

$\dot{Q}_{in,\alpha}^{l,t}(x_i)$ in Eq. (3) is calculated as

$$\dot{Q}_{in,\alpha}^{l,t}(x_i) = \frac{k_{r,\alpha}^{l-\frac{1}{2},t-1} K_{well}^{l-\frac{1}{2}}}{\mu_{\alpha}^{l-\frac{1}{2}}} \left(\frac{P_{B,sh}^{l-\frac{1}{2},t} - P_{T,sh}^{l-\frac{1}{2},t}}{h_{sh}^{l-\frac{1}{2}}} - \rho_{\alpha}^{l-\frac{1}{2}} g \right) \quad (10)$$

where $k_{r,\alpha}^{l-\frac{1}{2},t-1}$ is relative permeability of the phase α in shale layer $l-1/2$ at timestep $t-1$. $K_{well}^{l-\frac{1}{2}}$ is the effective absolute permeability of the well segment along layer $l-1/2$. $\mu_{\alpha}^{l-\frac{1}{2}}$ and $\rho_{\alpha}^{l-\frac{1}{2}}$ are viscosity and density of the phase α . $h_{sh}^{l-\frac{1}{2}}$ is the thickness of shale layer $l-1/2$. g is gravity

acceleration. $P_{B,sh}^{l-\frac{1}{2},t}$ is pressure at the bottom of shale layer $l-1/2$, and $P_{T,sh}^{l-\frac{1}{2},t}$ is pressure at the top of shale layer $l-1/2$ at timestep t . The subscript *sh* is used for shale.

$P_{B,sh}^{l-\frac{1}{2},t}$ and $P_{T,sh}^{l-\frac{1}{2},t}$ are considered same as those of the top of aquifer $l-1$ and the bottom of aquifer l , respectively. Thus,

$$\dot{Q}_{in,\alpha}^{l-1,t}(x_i) = \frac{k_{r,\alpha}^{l-\frac{1}{2},t-1} K_{well}^{l-\frac{1}{2}}}{\mu_\alpha^{l-\frac{1}{2}}} \left(\frac{P_{T,aq}^{l-1,t} - P_{B,aq}^{l,t}}{h_{sh}^{l-\frac{1}{2}}} - \rho_\alpha^{l-\frac{1}{2}} g \right) \quad (11)$$

$P_{T,aq}^{l-1,t}$ and $P_{B,aq}^{l,t}$ are expressed with the average pressure of the aquifer layers and pressure offset term, $F(l)$ as

$$\dot{Q}_{in,\alpha}^{l-1,t}(x_i) = \frac{k_{r,\alpha}^{l-\frac{1}{2},t-1} K_{well}^{l-\frac{1}{2}}}{\mu_\alpha^{l-\frac{1}{2}}} \left(\frac{(P_{aq}^{l-1,t} - F(l-1)) - (P_{aq}^{l,t} + F(l))}{h_{sh}^{l-\frac{1}{2}}} - \rho_\alpha^{l-\frac{1}{2}} g \right) \quad (12)$$

where

$$F(l) = \frac{S_\alpha^{l,t-1} \rho_\alpha^l + (1 - S_\alpha^{l,t-1}) \rho_\beta^l}{2} h_{aq}^l \quad (13)$$

$P_{aq}^{l-1,t}$ and $P_{aq}^{l,t}$ are vertically averaged pressure in aquifers $l-1$ and l , respectively, at timestep t .

Substituting Eq. (12) into Eq. (3),

$$\Delta P_{in,\alpha}^{l,t}(x_i) = \left(\frac{k_{r,\alpha}^{l-\frac{1}{2},t-1} K_{well}^{l-\frac{1}{2}}}{\mu_\alpha^{l-\frac{1}{2}} h_{sh}^{l-\frac{1}{2}}} P_{aq}^{l-1,t} - \frac{k_{r,\alpha}^{l-\frac{1}{2},t-1} K_{well}^{l-\frac{1}{2}}}{\mu_\alpha^{l-\frac{1}{2}} h_{sh}^{l-\frac{1}{2}}} P_{aq}^{l,t} - \frac{k_{r,\alpha}^{l-\frac{1}{2},t-1} K_{well}^{l-\frac{1}{2}}}{\mu_\alpha^{l-\frac{1}{2}} h_{sh}^{l-\frac{1}{2}}} F(l-1) - \frac{k_{r,\alpha}^{l-\frac{1}{2},t-1} K_{well}^{l-\frac{1}{2}}}{\mu_\alpha^{l-\frac{1}{2}} h_{sh}^{l-\frac{1}{2}}} F(l) - \frac{k_{r,\alpha}^{l-\frac{1}{2},t-1} K_{well}^{l-\frac{1}{2}}}{\mu_\alpha^{l-\frac{1}{2}}} \rho_\alpha^{l-\frac{1}{2}} g \right) * W_v(l) \quad (14)$$

where

$$W_v(l) = \frac{W(u)}{4\pi \Lambda_{h,aq}^{l,t-1} h_{aq}^l K_{h,aq}^l} \quad (15)$$

Similarly, $\Delta P_{in,\beta}^{l,t}(x_i)$, $\Delta P_{out,\alpha}^{l,t}(x_i)$, and $\Delta P_{out,\beta}^{l,t}(x_i)$ are calculated. And once they are substituted into Eq. (2), it becomes

$$\begin{aligned}
 \Delta P^{l,t}(x_i) = & \left(\frac{k_{r,\alpha}^{l-\frac{1}{2},t-1} K_{well}^{l-\frac{1}{2}}}{\mu_\alpha^{l-\frac{1}{2}} h_{sh}^{l-\frac{1}{2}}} P_{aq}^{l-1,t} - \frac{k_{r,\alpha}^{l-\frac{1}{2},t-1} K_{well}^{l-\frac{1}{2}}}{\mu_\alpha^{l-\frac{1}{2}} h_{sh}^{l-\frac{1}{2}}} P_{aq}^{l,t} - \frac{k_{r,\alpha}^{l-\frac{1}{2},t-1} K_{well}^{l-\frac{1}{2}}}{\mu_\alpha^{l-\frac{1}{2}} h_{sh}^{l-\frac{1}{2}}} F(l-1) - \frac{k_{r,\alpha}^{l-\frac{1}{2},t-1} K_{well}^{l-\frac{1}{2}}}{\mu_\alpha^{l-\frac{1}{2}} h_{sh}^{l-\frac{1}{2}}} F(l) \right. \\
 & \left. - \frac{k_{r,\alpha}^{l-\frac{1}{2},t-1} K_{well}^{l-\frac{1}{2}}}{\mu_\alpha^{l-\frac{1}{2}}} \rho_\alpha^{l-\frac{1}{2}} g \right) * W_v(l) \\
 & + \left(\frac{k_{r,\beta}^{l-\frac{1}{2},t-1} K_{well}^{l-\frac{1}{2}}}{\mu_\beta^{l-\frac{1}{2}} h_{sh}^{l-\frac{1}{2}}} P_{aq}^{l-1,t} - \frac{k_{r,\beta}^{l-\frac{1}{2},t-1} K_{well}^{l-\frac{1}{2}}}{\mu_\beta^{l-\frac{1}{2}} h_{sh}^{l-\frac{1}{2}}} P_{aq}^{l,t} - \frac{k_{r,\beta}^{l-\frac{1}{2},t-1} K_{well}^{l-\frac{1}{2}}}{\mu_\beta^{l-\frac{1}{2}} h_{sh}^{l-\frac{1}{2}}} F(l-1) - \frac{k_{r,\beta}^{l-\frac{1}{2},t-1} K_{well}^{l-\frac{1}{2}}}{\mu_\beta^{l-\frac{1}{2}} h_{sh}^{l-\frac{1}{2}}} F(l) \right. \\
 & \left. - \frac{k_{r,\beta}^{l-\frac{1}{2},t-1} K_{well}^{l-\frac{1}{2}}}{\mu_\beta^{l-\frac{1}{2}}} \rho_\beta^{l-\frac{1}{2}} g \right) * W_v(l) \\
 & + \left(\frac{k_{r,\alpha}^{l+\frac{1}{2},t-1} K_{well}^{l+\frac{1}{2}}}{\mu_\alpha^{l+\frac{1}{2}} h_{sh}^{l+\frac{1}{2}}} P_{aq}^{l,t} - \frac{k_{r,\alpha}^{l+\frac{1}{2},t-1} K_{well}^{l+\frac{1}{2}}}{\mu_\alpha^{l+\frac{1}{2}} h_{sh}^{l+\frac{1}{2}}} P_{aq}^{l+1,t} + \frac{k_{r,\alpha}^{l+\frac{1}{2},t-1} K_{well}^{l+\frac{1}{2}}}{\mu_\alpha^{l+\frac{1}{2}} h_{sh}^{l+\frac{1}{2}}} F(l) + \frac{k_{r,\alpha}^{l+\frac{1}{2},t-1} K_{well}^{l+\frac{1}{2}}}{\mu_\alpha^{l+\frac{1}{2}} h_{sh}^{l+\frac{1}{2}}} F(l+1) \right. \\
 & \left. - \frac{k_{r,\alpha}^{l+\frac{1}{2},t-1} K_{well}^{l+\frac{1}{2}}}{\mu_\alpha^{l+\frac{1}{2}}} \rho_\alpha^{l+\frac{1}{2}} g \right) * W_v(l) \\
 & + \left(\frac{k_{r,\beta}^{l+\frac{1}{2},t-1} K_{well}^{l+\frac{1}{2}}}{\mu_\beta^{l+\frac{1}{2}} h_{sh}^{l+\frac{1}{2}}} P_{aq}^{l,t} - \frac{k_{r,\beta}^{l+\frac{1}{2},t-1} K_{well}^{l+\frac{1}{2}}}{\mu_\beta^{l+\frac{1}{2}} h_{sh}^{l+\frac{1}{2}}} P_{aq}^{l+1,t} + \frac{k_{r,\beta}^{l+\frac{1}{2},t-1} K_{well}^{l+\frac{1}{2}}}{\mu_\beta^{l+\frac{1}{2}} h_{sh}^{l+\frac{1}{2}}} F(l) + \frac{k_{r,\beta}^{l+\frac{1}{2},t-1} K_{well}^{l+\frac{1}{2}}}{\mu_\beta^{l+\frac{1}{2}} h_{sh}^{l+\frac{1}{2}}} F(l+1) \right. \\
 & \left. - \frac{k_{r,\beta}^{l+\frac{1}{2},t-1} K_{well}^{l+\frac{1}{2}}}{\mu_\beta^{l+\frac{1}{2}}} \rho_\beta^{l+\frac{1}{2}} g \right) * W_v(l)
 \end{aligned} \tag{16}$$

Reorganizing Eq. (16),

$$\begin{aligned}
 \Delta P^{l,t}(x_i) = & \\
 W_v(l) * & \left[\left(\frac{k_{r,\alpha}^{l-\frac{1}{2},t-1} K_{well}^{l-\frac{1}{2}}}{\mu_\alpha^{l-\frac{1}{2}} h_{sh}^{l-\frac{1}{2}}} + \frac{k_{r,\beta}^{l-\frac{1}{2},t-1} K_{well}^{l-\frac{1}{2}}}{\mu_\beta^{l-\frac{1}{2}} h_{sh}^{l-\frac{1}{2}}} \right) P_{aq}^{l-1,t} - \left(\frac{k_{r,\alpha}^{l-\frac{1}{2},t-1} K_{well}^{l-\frac{1}{2}}}{\mu_\alpha^{l-\frac{1}{2}} h_{sh}^{l-\frac{1}{2}}} + \frac{k_{r,\beta}^{l-\frac{1}{2},t-1} K_{well}^{l-\frac{1}{2}}}{\mu_\beta^{l-\frac{1}{2}} h_{sh}^{l-\frac{1}{2}}} \right) P_{aq}^{l,t} \right. \\
 & - \left(\frac{k_{r,\alpha}^{l-\frac{1}{2},t-1} K_{well}^{l-\frac{1}{2}}}{\mu_\alpha^{l-\frac{1}{2}} h_{sh}^{l-\frac{1}{2}}} + \frac{k_{r,\beta}^{l-\frac{1}{2},t-1} K_{well}^{l-\frac{1}{2}}}{\mu_\beta^{l-\frac{1}{2}} h_{sh}^{l-\frac{1}{2}}} \right) F(l-1) \\
 & - \left. \left(\frac{k_{r,\alpha}^{l-\frac{1}{2},t-1} K_{well}^{l-\frac{1}{2}}}{\mu_\alpha^{l-\frac{1}{2}} h_{sh}^{l-\frac{1}{2}}} + \frac{k_{r,\beta}^{l-\frac{1}{2},t-1} K_{well}^{l-\frac{1}{2}}}{\mu_\beta^{l-\frac{1}{2}} h_{sh}^{l-\frac{1}{2}}} \right) F(l) \right. \\
 & \left. - K_{well}^{l-\frac{1}{2}} \mathcal{G} \left(\frac{k_{r,\alpha}^{l-\frac{1}{2},t-1}}{\mu_\alpha^{l-\frac{1}{2}}} \mathcal{Q}_\alpha^{l-\frac{1}{2}} + \frac{k_{r,\beta}^{l-\frac{1}{2},t-1}}{\mu_\beta^{l-\frac{1}{2}}} \mathcal{Q}_\beta^{l-\frac{1}{2}} \right) \right] \\
 + W_v(l) * & \left[\left(\frac{k_{r,\alpha}^{l+\frac{1}{2},t-1} K_{well}^{l+\frac{1}{2}}}{\mu_\alpha^{l+\frac{1}{2}} h_{sh}^{l+\frac{1}{2}}} + \frac{k_{r,\beta}^{l+\frac{1}{2},t-1} K_{well}^{l+\frac{1}{2}}}{\mu_\beta^{l+\frac{1}{2}} h_{sh}^{l+\frac{1}{2}}} \right) P_{aq}^{l,t} - \left(\frac{k_{r,\alpha}^{l+\frac{1}{2},t-1} K_{well}^{l+\frac{1}{2}}}{\mu_\alpha^{l+\frac{1}{2}} h_{sh}^{l+\frac{1}{2}}} + \frac{k_{r,\beta}^{l+\frac{1}{2},t-1} K_{well}^{l+\frac{1}{2}}}{\mu_\beta^{l+\frac{1}{2}} h_{sh}^{l+\frac{1}{2}}} \right) P_{aq}^{l+1,t} \right. \\
 & + \left(\frac{k_{r,\alpha}^{l+\frac{1}{2},t-1} K_{well}^{l+\frac{1}{2}}}{\mu_\alpha^{l+\frac{1}{2}} h_{sh}^{l+\frac{1}{2}}} + \frac{k_{r,\beta}^{l+\frac{1}{2},t-1} K_{well}^{l+\frac{1}{2}}}{\mu_\beta^{l+\frac{1}{2}} h_{sh}^{l+\frac{1}{2}}} \right) F(l) \\
 & + \left(\frac{k_{r,\alpha}^{l+\frac{1}{2},t-1} K_{well}^{l+\frac{1}{2}}}{\mu_\alpha^{l+\frac{1}{2}} h_{sh}^{l+\frac{1}{2}}} + \frac{k_{r,\beta}^{l+\frac{1}{2},t-1} K_{well}^{l+\frac{1}{2}}}{\mu_\beta^{l+\frac{1}{2}} h_{sh}^{l+\frac{1}{2}}} \right) F(l+1) \\
 & \left. - K_{well}^{l+\frac{1}{2}} \mathcal{G} \left(\frac{k_{r,\alpha}^{l+\frac{1}{2},t-1}}{\mu_\alpha^{l+\frac{1}{2}}} \mathcal{Q}_\alpha^{l+\frac{1}{2}} + \frac{k_{r,\beta}^{l+\frac{1}{2},t-1}}{\mu_\beta^{l+\frac{1}{2}}} \mathcal{Q}_\beta^{l+\frac{1}{2}} \right) \right]
 \end{aligned} \tag{17}$$

The initial pressure, $P_{aq}^{l,t=0}$, in each aquifer is set by the pressure gradient and depth, and as $\Delta P^{l,t}(x_i) = P_{aq}^{l,t} - P_{aq}^{l,t=0}$ in Eq. (1),

$$P_{aq}^{l,t} - P_{aq}^{l,t=0} =$$

$$W_v(l) * \left[C(l - \frac{1}{2})P_{aq}^{l-1,t} - C(l - \frac{1}{2})P_{aq}^{l,t} - C(l - \frac{1}{2})F(l - 1) - C(l - \frac{1}{2})F(l) - G(l - \frac{1}{2}) \right]$$

$$+ W_v(l) * \left[C(l + \frac{1}{2})P_{aq}^{l,t} - C(l + \frac{1}{2})P_{aq}^{l+1,t} + C(l + \frac{1}{2})F(l) + C(l + \frac{1}{2})F(l + 1) - G(l + \frac{1}{2}) \right]$$
(18)

where

$$C(l - \frac{1}{2}) = \frac{k_{r,\alpha}^{l-\frac{1}{2},t-1} K_{well}^{l-\frac{1}{2}}}{\mu_\alpha^{l-\frac{1}{2}} h_{sh}^{l-\frac{1}{2}}} + \frac{k_{r,\beta}^{l-\frac{1}{2},t-1} K_{well}^{l-\frac{1}{2}}}{\mu_\beta^{l-\frac{1}{2}} h_{sh}^{l-\frac{1}{2}}} = \frac{K_{well}^{l-\frac{1}{2}}}{h_{sh}^{l-\frac{1}{2}}} \left(\frac{k_{r,\alpha}^{l-\frac{1}{2},t-1}}{\mu_\alpha^{l-\frac{1}{2}}} + \frac{k_{r,\beta}^{l-\frac{1}{2},t-1}}{\mu_\beta^{l-\frac{1}{2}}} \right)$$

$$C(l + \frac{1}{2}) = \frac{k_{r,\alpha}^{l+\frac{1}{2},t-1} K_{well}^{l+\frac{1}{2}}}{\mu_\alpha^{l+\frac{1}{2}} h_{sh}^{l+\frac{1}{2}}} + \frac{k_{r,\beta}^{l+\frac{1}{2},t-1} K_{well}^{l+\frac{1}{2}}}{\mu_\beta^{l+\frac{1}{2}} h_{sh}^{l+\frac{1}{2}}} = \frac{K_{well}^{l+\frac{1}{2}}}{h_{sh}^{l+\frac{1}{2}}} \left(\frac{k_{r,\alpha}^{l+\frac{1}{2},t-1}}{\mu_\alpha^{l+\frac{1}{2}}} + \frac{k_{r,\beta}^{l+\frac{1}{2},t-1}}{\mu_\beta^{l+\frac{1}{2}}} \right)$$
(19)

$$C(l) = \frac{K_{well}^l}{h_{sh}^l} \left(\frac{k_{r,\alpha}^{l,t-1}}{\mu_\alpha^l} + \frac{k_{r,\beta}^{l,t-1}}{\mu_\beta^l} \right)$$

$$G(l - \frac{1}{2}) = K_{well}^{l-\frac{1}{2}} g \left(\frac{k_{r,\alpha}^{l-\frac{1}{2},t-1}}{\mu_\alpha^{l-\frac{1}{2}}} \varrho_\alpha^{l-\frac{1}{2}} + \frac{k_{r,\beta}^{l-\frac{1}{2},t-1}}{\mu_\beta^{l-\frac{1}{2}}} \varrho_\beta^{l-\frac{1}{2}} \right)$$

$$G(l + \frac{1}{2}) = K_{well}^{l+\frac{1}{2}} g \left(\frac{k_{r,\alpha}^{l+\frac{1}{2},t-1}}{\mu_\alpha^{l+\frac{1}{2}}} \varrho_\alpha^{l+\frac{1}{2}} + \frac{k_{r,\beta}^{l+\frac{1}{2},t-1}}{\mu_\beta^{l+\frac{1}{2}}} \varrho_\beta^{l+\frac{1}{2}} \right)$$
(20)

$$G(l) = K_{well}^l g \left(\frac{k_{r,\alpha}^{l,t-1}}{\mu_\alpha^l} \varrho_\alpha^l + \frac{k_{r,\beta}^{l,t-1}}{\mu_\beta^l} \varrho_\beta^l \right)$$

Reorganizing Eq. (18) with respect to pressure terms,

$$-W_v(l)C(l - \frac{1}{2})P_{aq}^{l-1,t} + \left(1 + W_v(l)C(l - \frac{1}{2}) - W_v(l)C(l + \frac{1}{2}) \right) P_{aq}^{l,t} + W_v(l)C(l + \frac{1}{2})P_{aq}^{l+1,t}$$

$$= W_v(l) * \left[-C(l - \frac{1}{2})F(l - 1) - C(l - \frac{1}{2})F(l) - G(l - \frac{1}{2}) + C(l + \frac{1}{2})F(l) \right.$$

$$\left. + C(l + \frac{1}{2})F(l + 1) - G(l + \frac{1}{2}) \right] + P_{aq}^{l,t=0}$$
(21)

Eq. (24) has a form of $(\mathbf{AA})(\mathbf{PP})=\mathbf{BB}$. The dimensions of \mathbf{AA} , \mathbf{PP} , and \mathbf{BB} are $(n-1)\times(n-1)$, $(n-1)\times 1$, and $(n-1)\times 1$, respectively, because it solves for aquifer 1 ($l=2$) through aquifer $n-1$ ($l=n$). \mathbf{AA} is a tridiagonal matrix, and it is solved using linear algebraic methods. Note that the calculated vector \mathbf{PP} is vertically averaged pressure in each aquifer, i.e., $P_{aq}^{l,t}(x_i)$. \mathbf{AA} and \mathbf{BB} are dependent on the CO_2 saturation from the previous step, and thus, Eq. (24) is built every timestep and calculated for \mathbf{PP} . Next, it computes the bottom and top pressure at each aquifer for flow calculation as

$$P_{aq,bottom}^{l,t}(x_i) = P_{aq}^{l,t}(x_i) + F(l) \quad l = 2, \dots, n \quad (25)$$

$$P_{aq,top}^{l,t}(x_i) = P_{aq}^{l,t}(x_i) - F(l) \quad l = 2, \dots, n \quad (26)$$

$F(l)$ is an offset term to consider pressure variation across aquifer l caused by gravity and fluid saturation as Eq. (13).

The pressure difference to calculate flow rate across shale layer $l-1/2$ is based on the top pressure of aquifer $l-1$ and the bottom pressure of aquifer l and as

$$\Delta P_{sh}^{l-\frac{1}{2},t}(x_i) = P_{aq,top}^{l-1,t}(x_i) - P_{aq,bottom}^{l,t}(x_i) \quad l = 2, \dots, n-1 \quad (27)$$

$$\Delta P_{sh}^{n-\frac{1}{2},t}(x_i) = P_{aq,top}^{n,t}(x_i) - P_{atm} \quad l = n$$

where P_{atm} is atmosphere pressure as described in Eq. (23).

Using Eq. (26) and Darcy's equation, the inflow mass rate (kg/s) of phase α into aquifer l is calculated as

$$\dot{Q}_{aq,\alpha}^{l,t}(x_i) = \frac{\pi(r_w^{l-\frac{1}{2}})^2 k_{r,\alpha}^{l-\frac{1}{2},t-1} K_{well}^{l-\frac{1}{2}} \left(\frac{\Delta P_{sh}^{l-\frac{1}{2},t}(x_i)}{h_{sh}^{l-\frac{1}{2}}} - \rho_\alpha^{l-\frac{1}{2}} g \right)}{\mu_\alpha^{l-\frac{1}{2}}} \quad l = 2, \dots, n \quad (28)$$

where r_w is the well radius in shale layer $l-1/2$.

Mass accumulation in aquifer l at timestep t is balance of inflow mass rate into aquifer l and outflow mass rate into aquifer $l+1$ out of aquifer l . Note that the outflow mass rate out of aquifer l is assumed to be entirely transported to aquifer $l+1$ through shale layer $l+1/2$ without any leakage into the shale layer, and is expressed as

$$M_{aq,\alpha}^{l,t} = \left(\dot{Q}_{aq,\alpha}^{l,t}(x_i) - \dot{Q}_{aq,\alpha}^{l+1,t}(x_i) \right) \times \Delta time \quad (29)$$

where $\dot{Q}_{aq,\alpha}^{l,t}(x_i)$ and $\dot{Q}_{aq,\alpha}^{l+1,t}(x_i)$ are respectively the inflow mass rate of the phase α into aquifer l and outflow mass rate out of aquifer l , which is the same as the inflow mass rate into aquifer $l+1$. $\Delta time$ is difference in time between current and previous timesteps. The MSW ROM

returns the inflow mass rate of each phase, $\dot{Q}_{aq,\alpha}^{l,t}(x_i)$, $\dot{Q}_{aq,\beta}^{l,t}(x_i)$, and cumulative mass amounts of phase α , $\Sigma M_{aq,\alpha}^l$.

The saturation, $S_\alpha^{l,t}$, at the leakage well in each aquifer is determined based on the cumulative mass amounts in aquifer l and Eqs. (4)-(7) in Baek et al. (2021). The value is used to calculate relative permeability and effective mobility in the next timestep.

3.0 Results and Discussion

This section presents a comparison of simulation results between the STOMP and MSW models and discusses the predictive capability of the MSW ROM in the context of quality assurance for use of the MSW ROM in the NRAP-Open-IAM. Following model validation against the numerical simulation reference results presented in Class et al. (2009), the performance of the MSW ROM as compared to STOMP simulations is investigated for two model geometries: one with a single overlying aquifer and one with four aquifers.

3.1 Model Validation

To evaluate the validity of the MSW ROM, we use a more detailed reservoir simulator, STOMP (White et al. 2012), which must be compared against a reference calculation of other simulators and tools. To do this, we developed a STOMP model based on a well-documented literature case study (geometry presented in Figure 2). Class et al. (2009) conducted a comparison study among multiple institutes using multiple numerical simulation tools but with the same geology and fluid models. This benchmark study provides a widely referenced test case. On Figure 4, the leakage rate on the y-axis indicates the relative mass rate of CO₂ leaked into aquifer 1 with respect to the injected mass rate as in Eq. (30), and our STOMP result is compared with the reference simulations (Class et al. 2009). Good agreement with other codes (Figure 4) provides confidence in the numerical model, as used in this report, to provide a reference model to build a reservoir lookup table and for the validation by comparison with the two cases with different aquifer stratigraphy.

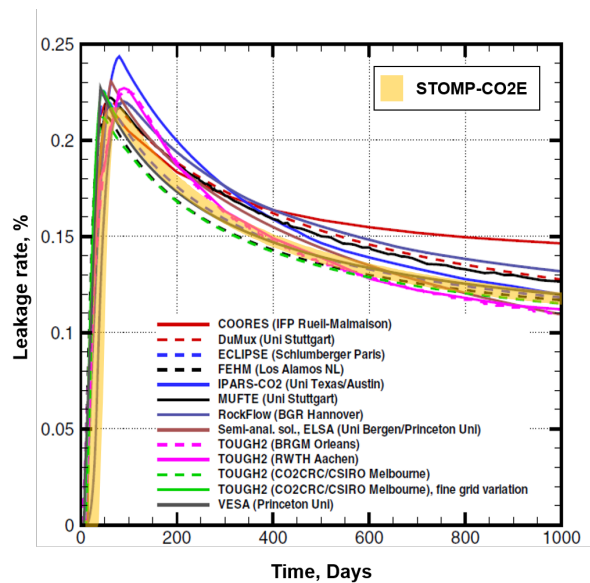


Figure 4. Validation of STOMP model.

$$Leakage\ rate,\ % = \frac{Leakage\ mass\ rate\ of\ CO_2\ into\ aquifer\ 1}{Injection\ mass\ rate\ into\ reservoir} \times 100 \tag{30}$$

Next, the MSW ROM is built based on the benchmark problem (Class et al. 2009). Figure 5 compares the mass rates of brine (Figure 5a) and CO₂ leakage (Figure 5b) from the storage reservoir into the overlying aquifer 1 (Figure 2a) for two versions of the MSW ROM (original: asterisks and modified: empty circles) and STOMP results. The original MSW ROM was implemented up to version alpha 2.3.2 of the NRAP-Open-IAM, and it is updated through this study. Also shown on Figure 5 (right-side y-axis) is the absolute difference between the analytic and numerical models. For brine, the MSW ROM results (blue and red) in Figure 5a show good matching up to 100 days. During CO₂ injection operation, once CO₂ reaches the leaky well and in-place mobile brine is displaced entirely (after 100 days), no more brine is leaked from the reservoir. For CO₂, there is an increase in the leakage rate over time up to 50 days (blue and red) in Figure 5b, and the reduction afterward is attributed to the constant pressure boundary condition applied. The present study (red) modified the original MSW ROM (blue) and improved the accuracy. The modified model shows improved matching to the numerical simulation results for both brine and CO₂ over the entire 1,000-day simulation period.

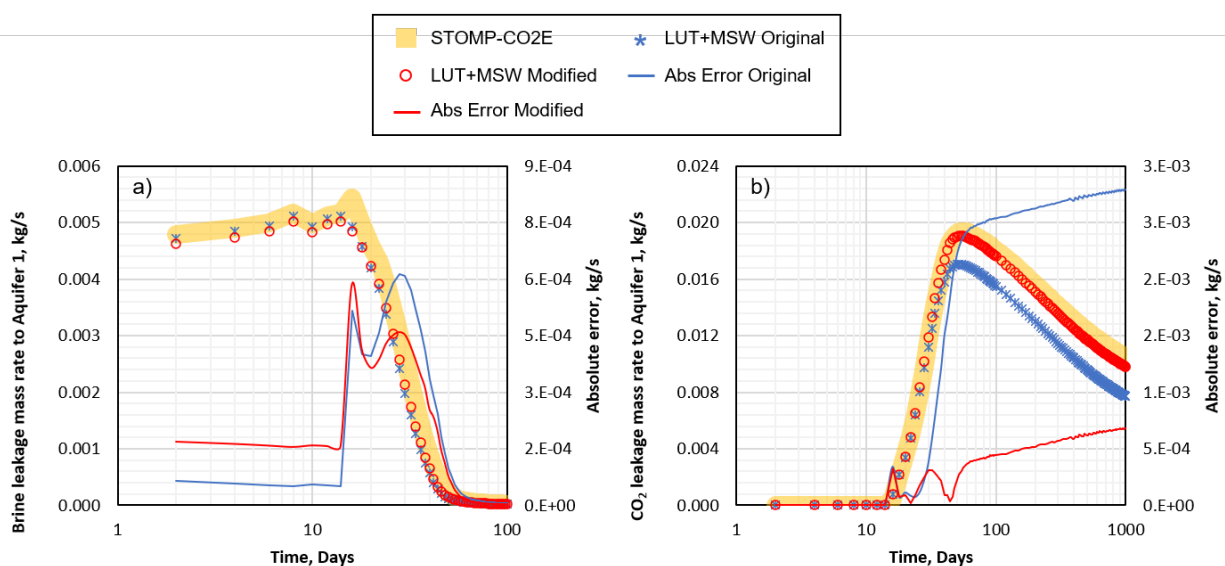


Figure 5. Coupled MSW ROM validation against STOMP results: a) brine leakage mass rate into aquifer 1 from the storage reservoir; b) CO₂ leakage mass rate into aquifer 1 from the storage reservoir. STOMP-CO₂E result (yellow) on the right subplot is identical to that in Figure 4. Log time is used for both x-axes. The NRAP model (i.e., MSW ROM) is shown in red (modified version) and blue (original version). The secondary y-axis (right side) calculates the absolute difference.

3.2 Multiple Layer Model Applications

The MSW ROM in the NRAP-Open-IAM is designed to study more complex models with a user-defined number of aquifers and shales. In this section, the wellbore model is applied to a geological model with four aquifers and five shale layers as shown in Figure 6. The parameters are the same as those in Table 1 except for the total number of aquifers and shale layers and residual brine saturation in each aquifer. Residual brine saturation is set according to the values presented in Table 2. Leakage into the atmosphere can be calculated in the model in the same way to that for aquifers, but here it is not considered by setting the permeability of the well segment across shale 5 very small (ca. 10^{-99} m²). The STOMP model's geology and residual brine saturation values are modified accordingly and run to generate the lookup table for the reservoir layer and for comparison with the analytical approach.

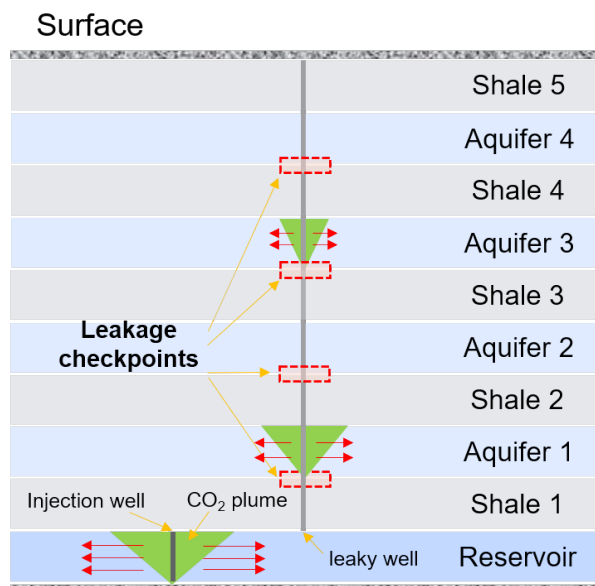


Figure 6. Multiple layer model with four aquifers and five shale layers.

Table 2. Residual brine saturation used for the multiple layer model.

Parameter	Units	Value
Residual brine saturation in aquifer 1	-	0.18
Residual brine saturation in aquifer 2	-	0.40
Residual brine saturation in aquifer 3	-	0.50
Residual brine saturation in aquifer 4	-	0.00

Figure 7 compares the inflow mass rate of each phase in each aquifer from the NRAP analytical calculation, Eq. (28), with those of the numerical STOMP simulation. For both phases of the fluids, the result matches well overall except during the early transient period before 200 days. During the early time, the pressure and saturation in each aquifer are perturbed by the fluid leakage through the well, and later each aquifer reaches steady-state condition. This is reasonable accuracy considering the purpose of the analytical model and its simplicity.

Cumulative mass of the leaked CO_2 in each aquifer is calculated as output of the NRAP model using Eq. (29). As expected from the good matching in the inflow mass rate in Figure 7, the cumulative mass for all aquifers is matching well to the numerical simulation results over time (Figure 8).

Note that the MSW model needs specification of a non-zero residual brine saturation, in that the maximum CO_2 saturation in each aquifer must be less than one, to simulate the impact of horizontal leakage in each aquifer, which may lead to a reduction in the leakage of CO_2 out of the aquifers through the wells. This approach is qualitatively in agreement with the approach described in Nordbotten et al. (2009). The default residual brine saturation is set to zero, which is a conservative consideration for risk assessment of CO_2 leakage (i.e., over estimates the amount that may leak). The MSW ROM uses three shale layers and two aquifers as the default setting, and the result for the default case (i.e., two aquifers model) is included in Appendix B.

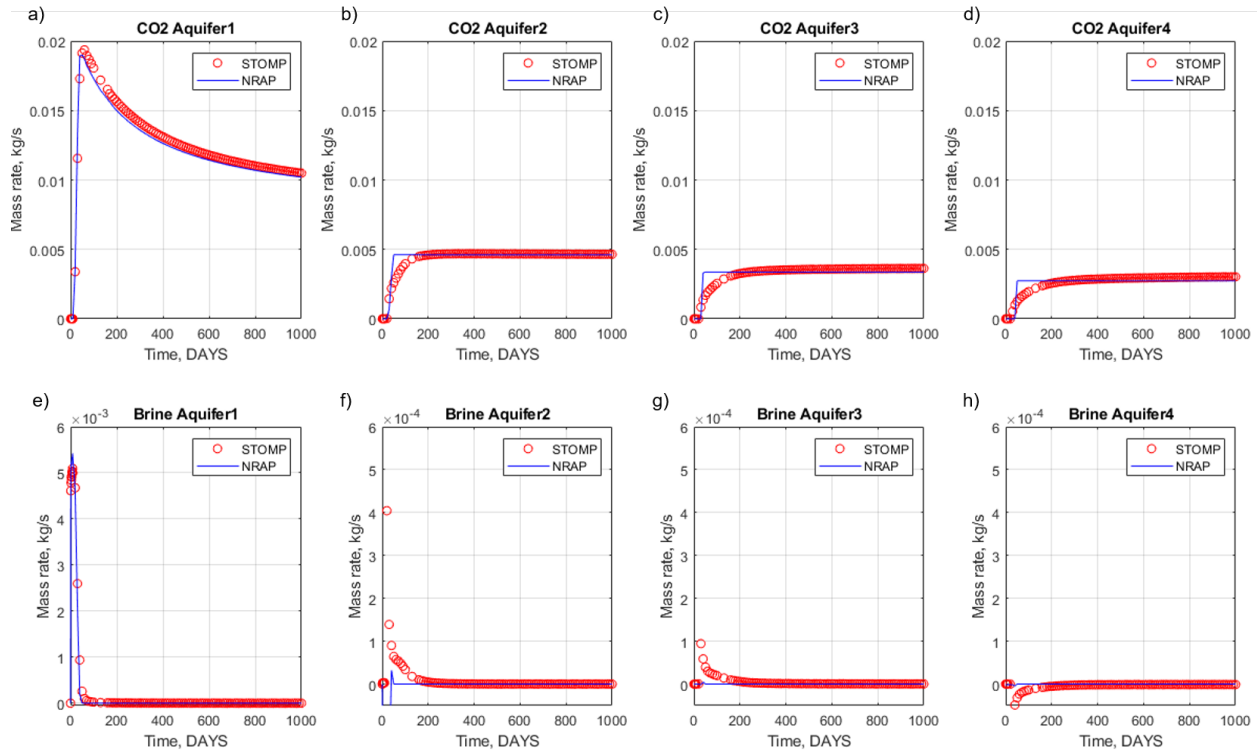


Figure 7. Inflow mass rate comparison. Red: STOMP, blue: NRAP. Top row: CO₂, bottom row: brine.

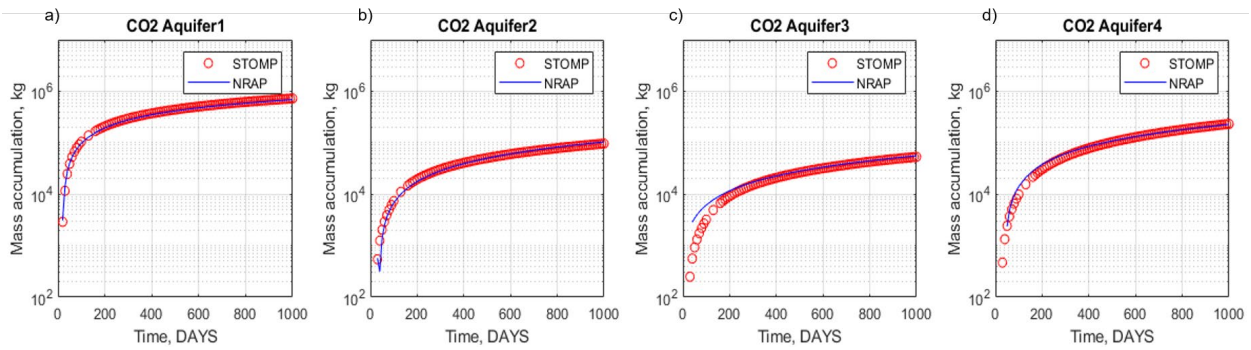


Figure 8. Cumulative mass comparison. Red: STOMP, blue: NRAP.

4.0 Conclusion

This report presents the testing of MSW ROM in NRAP-Open-IAM. For validation, numerical simulation models were built using STOMP and based on a benchmark problem (Class et al. 2009). This model is also the basis for the reservoir lookup table model, which feeds the numerical simulation information on dynamic reservoir behavior to the MSW ROM. The wellbore ROM predicts the leakage of CO₂ and brine from a storage reservoir to one or more overlying aquifers.

The results show that the modified MSW ROM predicts the leakage of the two-phase fluids well over time when compared to the numerical calculation for the single aquifer model (Figure 2). For the multiple aquifers model (Figure 6), it is observed that the model needs site-specific inputs of the residual brine saturation in each aquifer. The appropriate assumption for the residual saturation leads to reasonable prediction in the leakage rate and mass accumulation. This parameter can be considered one of the uncertain parameters requiring stochastic analysis, which is part of the NRAP-Open-IAM capabilities. The default setting of no residual brine saturation ensures a conservative leakage risk assessment.

The developed wellbore ROM effectively embraces underlying uncertainties associated with the leakage through abandoned wells for the risk assessment. Coupled with other component models such as the reservoir models and aquifer impact models, this wellbore model has broad applicability for practical risk assessment in GCS operations.

5.0 References

- Baek S, DH Bacon, and N Huerta. 2021. *NRAP-Open-IAM Analytical Reservoir Model Development and Testing*. PNNL-31418, Pacific Northwest National Laboratory, Richland, WA.
- Bacon DH, L Pan, and CM Oldenburg. 2021. *NRAP-Open-IAM: Open Wellbore Component v2.0*. PNNL-31543, Pacific Northwest National Laboratory, Richland, WA.
- Bacon DH, DI Demirkanli, and SK White. 2020. "Probabilistic risk-based Area of Review (AoR) determination for a deep-saline carbon storage site." *International Journal of Greenhouse Gas Control* 102(November):103153. <https://doi.org/10.1016/j.ijggc.2020.103153>
- Bear J. 1979. *Hydraulics of Groundwater*. McGraw-Hill, New-York.
- Class H, A Ebigbo, R Helmig, HK Dahle, JM Nordbotten, MA Celia, P Audigane, M Darcis, J Ennis-King, Y Fan, B Flemisch, SE Gasda, M Jin, S Krug, D Labregere, AN Beni, RJ Pawar, A Sbai, SG Thomas, L Trenty, and L Wei. 2009. "A benchmark study on problems related to CO₂ storage in geologic formations." *Computers & Geosciences* 13(July):409-434. <https://doi.org/10.1007/s10596-009-9146-x>
- Gasda SE, S Bachu, and MA Celia. 2004. "Spatial characterization of the location of potentially leaky wells penetrating a deep saline aquifer in a mature sedimentary basin." *Environmental Geology*. 46(October):707–720. <https://doi.org/10.1007/s00254-004-1073-5>
- Jordan AB, PH Stauffer, D Harp, JW Carey, and RJ Pawar. 2015. "A response surface model to predict CO₂ and brine leakage along cemented wellbores." *International Journal of Greenhouse Gas Control* 33:27-39. <http://dx.doi.org/10.1016/j.ijggc.2014.12.002>
- Nordbotten JM, MA Celia, and S. Bachu. 2004. "Analytical solutions for leakage rates through abandoned wells." *Water Resources Research* 40(April):W04204. <https://doi.org/10.1029/2003WR002997>
- Nordbotten JM, MA Celia, and S. Bachu. 2009. "Model for CO₂ Leakage Including Multiple Geological Layers and Multiple Leaky Wells." *Environmental Science & Technology* 43(December):743-749. <https://doi.org/10.1021/es801135v>
- Nordbotten JM and MA Celia. 2012. *Geological Storage of CO₂ Modeling Approaches for Large-Scale Simulation*. Wiley, New York.
- NETL (National Energy Technology Laboratory). 2021. NRAP-Open-IAM. Accessed May 26, 2021. <https://qitlab.com/NRAP/OpenIAM>
- Peaceman DW. 1983. "Interpretation of Well-Block Pressures in Numerical Reservoir Simulation with Non-Square Grid Blocks and Anisotropic Permeability." *Society of Petroleum Engineers Journal* 23(3):531-543. <https://doi.org/10.2118/10528-Pa>
- Pawar R, R Dilmore, S Chu, Y Zhang, C Oldenburg, P Stauffer, G Guthrie, and G Bromhal. 2016. "Informing Geologic CO₂ Storage Site Management Decisions under Uncertainty: Demonstration of NRAP's Integrated Assessment Model (NRAP-IAM-CS) Application." *Energy Procedia* 114(July):4330-4337. <https://doi.org/10.1016/j.egypro.2017.03.1582>

Vasylykivska V, R Dilmore, G Lackey, Y Zhang, S King, D Bacon, B Chen, K Mansoor, and D Harp. 2021. "NRAP-open-IAM: A flexible open-source integrated-assessment-model for geologic carbon storage risk assessment and management." *Environmental Modelling & Software* 143(September):105114. <https://doi.org/10.1016/j.envsoft.2021.105114>

White MD, DJ Watson, DH Bacon, SK White, BP McGrail, and ZF Zhang. 2012. *STOMP Subsurface Transport Over Multiple Phases. STOMP-CO2 and -CO2e Guide*. PNNL-21268, Pacific Northwest National Laboratory, Richland, WA.

Yonkofski C, G Tartakovsky, N Huerta, and A Wentworth. 2019. "Risk-based monitoring designs for detecting CO2 leakage through abandoned wellbores: An application of NRAP's WLAT and DREAM tools." *International Journal of Greenhouse Gas Control* 91(December):102807. <https://doi.org/10.1016/j.ijggc.2019.102807>

Appendix A – Input file of STOMP for a Benchmark Problem

The STOMP input for the benchmark problem (Ebigbo et al. 2007) is provided below to enable users to reproduce our modeling.

```

## Start of Input
1    ~Simulation Title Card
2    1,
3    STOMP Example Problem CO2E-1,
4    Mark White,
5    Pacific Northwest Laboratory,
6    01 June 2011,
7    09:37 PDT,
8    1,
9    Generated by Diana H. Bacon and Seunghwan Baek, Jun-21-2021
10
11   ~Solution Control Card
12   Normal,
13   STOMP-CO2e Isothermal w/ Invariant Fluid Density and Viscosity,
14   1,
15   0,day,1000,day,1,s,10,day,1.25,16,1.e-06,0.001,s,0.2,
16   167,hr,167,hr,99999,
17   Variable Aqueous Diffusion,
18   Variable Gas Diffusion,
19   1045,kg/m^3,2.535e-4,Pa s,479,kg/m^3,3.95e-5,Pa s,
20   0,
21
22   ~Grid Card
23   Cartesian,
24   73,73,23,
25   -500.000,m,-475.000,m,-450.000,m,-425.000,m,-400.000,m,-375.000,m,
26   -350.000,m,-325.000,m,-300.000,m,-275.000,m,-255.000,m,-235.000,m,
27   -215.000,m,-200.000,m,-185.000,m,-170.000,m,-160.000,m,-150.000,m,
28   -140.000,m,-130.000,m,-122.500,m,-115.000,m,-107.500,m,-102.500,m,
29   -97.500,m,-92.500,m,-85.000,m,-77.500,m,-70.000,m,-60.000,m,
30   -50.000,m,-40.000,m,-30.000,m,-20.000,m,-12.500,m,-8.000,m,
31   -5.000,m,-2.800,m,-1.500,m,-0.800,m,-0.400,m,-0.133,m,
32   0.133,m,0.400,m,0.800,m,1.500,m,2.800,m,5.000,m,
33   8.000,m,12.500,m,20.000,m,30.000,m,40.000,m,50.000,m,
34   60.000,m,70.000,m,85.000,m,100.000,m,125.000,m,150.000,m,
35   175.000,m,200.000,m,225.000,m,250.000,m,275.000,m,300.000,m,
36   325.000,m,350.000,m,375.000,m,400.000,m,425.000,m,450.000,m,
37   475.000,m,500.000,m,
38   -500.000,m,-475.000,m,-450.000,m,-425.000,m,-400.000,m,-375.000,m,
39   -350.000,m,-325.000,m,-300.000,m,-275.000,m,-255.000,m,-235.000,m,
40   -215.000,m,-200.000,m,-185.000,m,-170.000,m,-160.000,m,-150.000,m,
41   -140.000,m,-130.000,m,-122.500,m,-115.000,m,-107.500,m,-102.500,m,
42   -97.500,m,-92.500,m,-85.000,m,-77.500,m,-70.000,m,-60.000,m,
43   -50.000,m,-40.000,m,-30.000,m,-20.000,m,-12.500,m,-8.000,m,
44   -5.000,m,-2.800,m,-1.500,m,-0.800,m,-0.400,m,-0.133,m,
45   0.133,m,0.400,m,0.800,m,1.500,m,2.800,m,5.000,m,
46   8.000,m,12.500,m,20.000,m,30.000,m,40.000,m,50.000,m,
47   60.000,m,70.000,m,85.000,m,100.000,m,125.000,m,150.000,m,
48   175.000,m,200.000,m,225.000,m,250.000,m,275.000,m,300.000,m,

```

49	325.000,m,350.000,m,375.000,m,400.000,m,425.000,m,450.000,m,
50	475.000,m,500.000,m,
51	0.0,m,4.41,m,8.32,m,11.80,m,14.90,m,17.65,m,20.09,m,22.27,m,24.20,m,
52	25.92,m,27.44,m,28.80,m,30.0,m,
53	1@100.000,m,
54	10@3.000,m,
55	
56	~Inactive Nodes Card
57	4,
58	1,41,1,73,13,13,
59	43,73,1,73,13,13,
60	42,42,1,41,13,13,
61	42,42,43,73,13,13,
62	
63	~Rock/Soil Zonation Card
64	3,
65	reservoir,1,73,1,73,1,23,
66	aquifer,1,73,1,73,14,23,
67	grout,42,42,42,42,1,23,
68	
69	~Mechanical Properties Card
70	reservoir,2650,kg/m^3,0.15,0.15,Compressibility,1.e-8,1/psi,,,constant,1.0,1.0,
71	aquifer,2650,kg/m^3,0.15,0.15,Compressibility,1.e-8,1/psi,,,constant,1.0,1.0,
72	grout,2650,kg/m^3,0.15,0.15,Compressibility,1.e-8,1/psi,,,constant,1.0,1.0,
73	
74	~Hydraulic Properties Card
75	reservoir,2.e-14,m^2,2.e-14,m^2,2.e-14,m^2,
76	aquifer,2.e-14,m^2,2.e-14,m^2,2.e-14,m^2,
77	grout,1.e-12,m^2,1.e-12,m^2,1.e-12,m^2,
78	
79	~Saturation Function Card
80	reservoir,Brooks and Corey,0.01,m,1.0,,,
81	aquifer,Brooks and Corey,0.01,m,1.0,,,
82	grout,Brooks and Corey,0.01,m,1.0,,,
83	
84	~Aqueous Relative Permeability Card
85	reservoir,tabular,2,
86	0.0,0.0,
87	1.0,1.0,
88	aquifer,tabular,2,
89	0.0,0.0,
90	1.0,1.0,
91	grout,tabular,2,
92	0.0,0.0,
93	1.0,1.0,
94	
95	~Gas Relative Permeability Card
96	reservoir,tabular,2,
97	0.0,0.0,
98	1.0,1.0,
99	aquifer,tabular,2,
100	0.0,0.0,
101	1.0,1.0,
102	grout,tabular,2,
103	0.0,0.0,
104	1.0,1.0,

105
 106 ~Salt Transport Card
 107 reservoir,0.0,ft,0.0,ft,
 108 aquifer,0.0,ft,0.0,ft,
 109 grout,0.0,ft,0.0,ft,
 110
 111 ~Initial Conditions Card
 112 Hydrostatic,30.7534,MPa,0,m,34,C,0,m,0,C/m,0.0,0,m,0,1/m,
 113
 114 ~Boundary Conditions Card
 115 4,
 116 West,Aqu. Initial Condition,Gas Initial Condition,Aqu. Mass Frac.,
 117 1,1,1,73,1,23,1,
 118 0,s,,,,,0.0,,,,
 119 East,Aqu. Initial Condition,Gas Initial Condition,Aqu. Mass Frac.,
 120 73,73,1,73,1,23,1,
 121 0,s,,,,,0.0,,,,
 122 North,Aqu. Initial Condition,Gas Initial Condition,Aqu. Mass Frac.,
 123 1,73,73,73,1,23,1,
 124 0,s,,,,,0.0,,,,
 125 South,Aqu. Initial Condition,Gas Initial Condition,Aqu. Mass Frac.,
 126 1,73,1,1,1,23,1,
 127 0,s,,,,,0.0,,,,
 128
 129 ~Coupled Well Card
 130 1,
 131 CO2 Injection Well,Water Relative Saturation,1.0,1.0,1.0,1,MMT,
 132 1,
 133 -100.0,m,0,m,30.0,m,-100.0,m,0,m,0.0,m,0.15,m,0.0,screened,
 134 1,
 135 0.0,hr,8.87,kg/s,45,MPa,0.0,
 136
 137 ~Output Options Card
 138 11,
 139 42,42,1,
 140 42,42,6,
 141 42,42,7,
 142 42,42,12,
 143 42,42,13,
 144 42,42,14,
 145 42,42,16,
 146 42,42,18,
 147 42,42,20,
 148 42,42,22,
 149 42,42,23,
 150 1,1,day,m,6,6,6,
 151 18,
 152 Phase Condition,,
 153 Gas Saturation,,
 154 Gas Relative Permeability,,
 155 #Trapped Gas Saturation,,
 156 Integrated CO2 Mass,kg,
 157 Integrated CO2 Aqueous Mass,kg,
 158 Integrated CO2 Gas Mass,kg,
 159 Integrated CO2 Trapped-Gas Mass,kg,
 160 Salt Aqueous Mass Fraction,,

```

161 CO2 Aqueous Mass Fraction,,
162 Gas Density,kg/m^3,
163 Aqueous Density,kg/m^3,
164 Gas Viscosity,Pa s,
165 Aqueous Viscosity,Pa s,
166 Gas Pressure,MPa,
167 Aqueous Pressure,MPa,
168 #Diffusive Porosity,,
169 Coupled-Well Press,1,MPa,
170 Coupled-Well CO2 Mass Rate,1,kg/s,
171 Coupled-Well CO2 Mass Integral,1,kg,
172 1,
173 100@10.0,day,
174 17,
175 Rock/Soil Type,,
176 Gas Saturation,,
177 Trapped Gas Saturation,,
178 Salt Saturation,,
179 CO2 Aqueous Concentration,gm/cm^3,
180 Salt Aqueous Mass Fraction,,
181 CO2 Aqueous Mass Fraction,,
182 Gas Pressure,MPa,
183 Aqueous Pressure,MPa,
184 Diffusive Porosity,,
185 Gas Density,kg/m^3,
186 Aqueous Density,kg/m^3,
187 Phase Condition,,
188 x-direction node centroid,ft,
189 y-direction node centroid,ft,
190 z-direction node centroid,ft,
191 No restart,,
192
193 ~Surface Flux Card
194 2,
195 CO2 Mass Flux,kg/s,kg,top,42,42,42,42,13,13,
196 Aqueous Mass Flux,kg/s,kg,top,42,42,42,42,13,13,

## End of Input

```

Figure A.1. Input file of STOMP for a benchmark problem (Ebigbo et al. 2007)

Appendix B – Case Study with the Default Number of Aquifers

The multisegmented wellbore reduced-order model (MSW ROM) uses three shale layers and two aquifers as default setting, and the result for the default case (i.e., two aquifers model) is shown in Figure B.1.

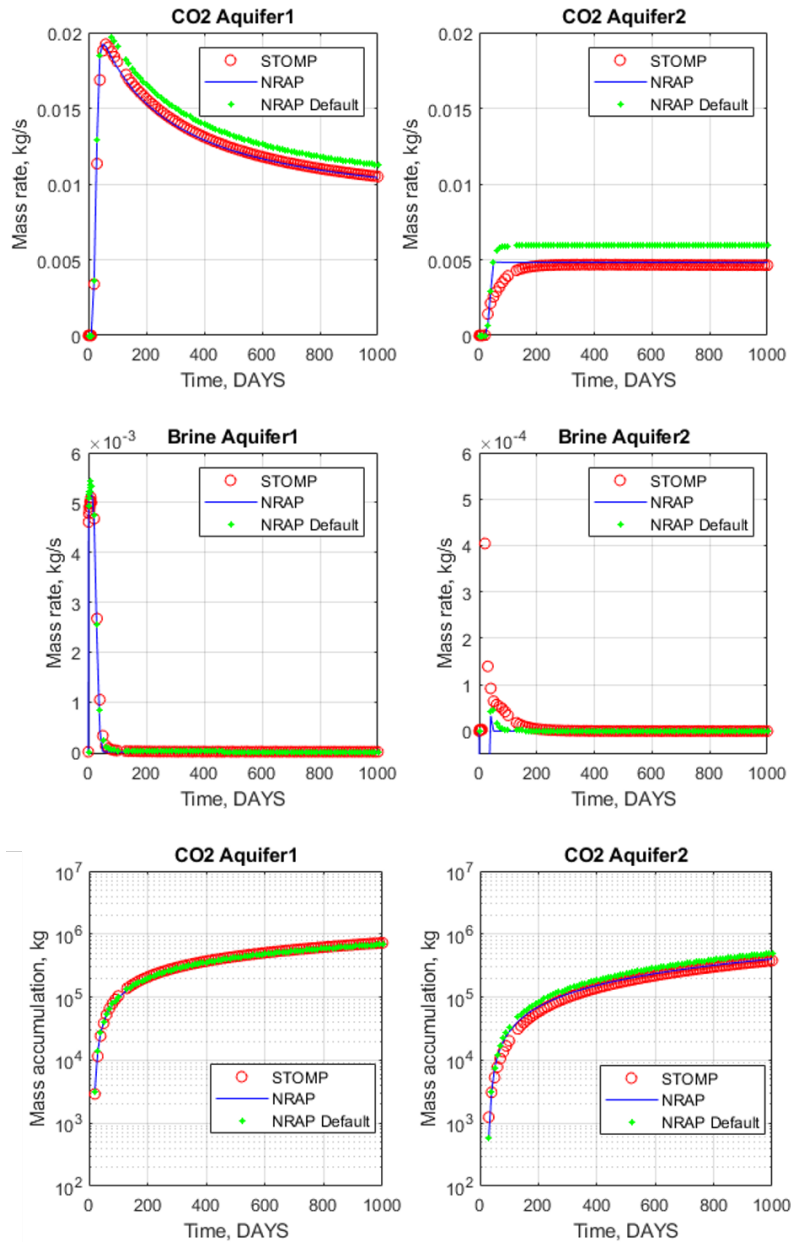


Figure B.1. Impacts of the residual brine saturation on MSW ROM outputs for the two aquifers model. Top panels: inflow CO₂ mass rate. Middle panels: inflow brine mass rate. Bottom panels: CO₂ mass accumulation. Red: STOMP. Blue: MSW ROM with residual brine saturation in Table B.1. Green: MSW ROM with default residual brine saturation (i.e., zero in all aquifers).

Table B.1. Residual brine saturation used for the two aquifers model.

Parameter	Units	Value
Residual brine saturation in reservoir	-	0.08
Residual brine saturation in aquifer 1	-	0.15
Residual brine saturation in aquifer 2	-	0.00

Mean absolute error (MAE) is calculated as

$$\text{Mean absolute error (MAE)} = \frac{\sum_{i=1}^{n_T} |X_{i,MSW} - X_{i,STOMP}|}{n_T} \quad (\text{B.1})$$

$X_{i,MSW}$ are results of MSW, which are CO₂ inflow mass rate, kg/s, brine inflow mass rate or CO₂ mass accumulation, kg. Likewise, $X_{i,STOMP}$ are results of STOMP. MAE is calculated for each aquifer based on Eq. (B.1), and the result is compared with the default case in Table B.2.

Table B.2. Impacts of residual brine saturation on MAE for MSW ROM outputs.

MAE Targets	Unit	Aquifer 1	Aquifer 2	Aquifer 1, default	Aquifer 2, default
Inflow CO ₂ mass rate	kg/s	1.8955e-04	2.4844e-04	7.6617e-04	12.0213e-04
Inflow brine mass rate	kg/s	4.7788e-05	1.8772e-05	3.4854e-05	1.7906e-05
CO ₂ mass accumulation	kg	1.9515e+04	1.3838e+04	1.8543e+04	5.4283e+04

Pacific Northwest National Laboratory

902 Battelle Boulevard
P.O. Box 999
Richland, WA 99354
1-888-375-PNNL (7665)

www.pnnl.gov